PNAS RESEARCH ARTICLE | PHYSIOLOGY

Capillary oxygen regulates demand–supply coupling by triggering connexin40-mediated conduction: Rethinking the metabolic hypothesis

Paulina M. Kowalewska[a,b,1], Stephanie L. Milkovich[a], Daniel Goldman[c], Shaun L. Sandow[d,e], Christopher G. Ellis[a,c], and Donald G. Welsh[a,b]

Edited by M. Celeste Simon, University of Pennsylvania Perelman School of Medicine, Philadelphia, PA; received February 26, 2023; accepted December 21, 2023

Coupling red blood cell (RBC) supply to O_2 demand is an intricate process requiring O_2 sensing, generation of a stimulus, and signal transduction that alters upstream arteriolar tone. Although actively debated, this process has been theorized to be induced by hypoxia and to involve activation of endothelial inwardly rectifying K^+ channels (K_{IR}) 2.1 by elevated extracellular K^+ to trigger conducted hyperpolarization via connexin40 (Cx40) gap junctions to upstream resistors. This concept was tested in resting healthy skeletal muscle of *Cx40*$^{-/-}$ and endothelial *K*$_{IR}$*2.1*$^{-/-}$ mice using state-of-the-art live animal imaging where the local tissue O_2 environment was manipulated using a custom gas chamber. Second-by-second capillary RBC flow responses were recorded as O_2 was altered. A stepwise drop in PO_2 at the muscle surface increased RBC supply in capillaries of control animals while elevated O_2 elicited the opposite response; capillaries were confirmed to express Cx40. The RBC flow responses were rapid and tightly coupled to O_2; computer simulations did not support hypoxia as a driving factor. In contrast, RBC flow responses were significantly diminished in *Cx40*$^{-/-}$ mice. Endothelial *K*$_{IR}$*2.1*$^{-/-}$ mice, on the other hand, reacted normally to O_2 changes, even when the O_2 challenge was targeted to a smaller area of tissue with fewer capillaries. Conclusively, microvascular O_2 responses depend on coordinated electrical signaling via Cx40 gap junctions, and endothelial $K_{IR}2.1$ channels do not initiate the event. These findings reconceptualize the paradigm of blood flow regulation in skeletal muscle and how O_2 triggers this process in capillaries independent of extracellular K^+.

conduction | erythrocyte | intravital microscopy | microcirculation | oxygen transport

Red blood cell (RBC) flow through the microvasculature is intimately matched to tissue O_2 requirements. At a fundamental level, O_2 demand–supply coupling entails sensing of the O_2 need and generation of a stimulus that alters arteriolar tone—the primary locus of blood flow control. Under the classical metabolic hypothesis, sensing occurs in parenchyma where tissue activity and induction of hypoxia drive the accumulation of vasoactive metabolites (1) and ions, such as K^+, which activates inwardly rectifying K^+ channels (K_{IR}) to initiate arteriolar dilation (2). While this "textbook" explanation is simple to rationalize, a system built on hypoxic production of metabolites and ions along with their diffusional spread is difficult to square with the necessity for precise temporal and spatial control (3, 4). As such, a counternarrative diverging from a focus on arterioles and tissue mitochondria to that of capillaries and RBCs is gaining traction (5, 6).

The idea that the microcirculation rather than the parenchyma sense O_2 is an appealing concept, but one difficult to validate (7) as it requires 1) manipulation of RBC O_2, 2) dynamic measures of capillary hemodynamics, and 3) experimentation where outcomes separate classic thinking from emerging counternarratives. In this regard, we established key technology: a gas-exchange chamber that enables in vivo imaging of the capillary circulation while tissue/RBC O_2 kinetics are manipulated (8, 9). Software development has in turn automated microhemodynamic analysis such that RBC flow and hemoglobin O_2 saturation (SO_2) can be assessed over large subsets of capillaries (10). With these innovations in place, genetic deletion models targeting key proteins can be used to probe unresolved concepts of O_2 demand–supply coupling.

Herein, this study used state-of-the-art intravital imaging (Fig. 1) and analytical approaches (*SI Appendix*, Fig. S1) to probe the O_2 regulatory system in healthy resting skeletal muscle, the extensor digitorum longus (EDL). Experiments were first designed to test whether the signals driving demand–supply coupling originate in capillaries (9) and conduct via interendothelial gap junctions composed of connexin40 (Cx40) (11). Experiments next addressed whether, in accordance with the metabolic hypothesis, the "signal" involves tissue release of K^+ (12), whose extracellular rise activates endothelial cell (EC) $K_{IR}2.1$ (13, 14). Results show

Significance

Matching oxygen supply to tissue demand is a vital process achieved by fine adjustments in microvascular red blood cell flow. How these responses are triggered and communicated in microvascular networks of skeletal muscle is currently debated. A potential mechanism involves activation of potassium-sensitive channels by extracellular potassium, leading to arterial hyperpolarization and vasodilation. Using a customized experimental setup, we show that capillary communication with arterioles occurs via signals that spread through gap junctions composed of Cx40 (connexin40) to match red blood cell flow to oxygen needs in skeletal muscle. These responses are not triggered by hypoxia or extracellular potassium. These findings advance the mechanistic understanding of oxygen demand–supply coupling in skeletal muscle.

Author contributions: P.M.K., D.G., C.G.E., and D.G.W. designed research; P.M.K., S.L.M., and S.L.S. performed research; D.G., S.L.S., C.G.E., and D.G.W. contributed new reagents/analytic tools; P.M.K., S.L.M., and D.G. analyzed data; S.L.M., D.G., S.L.S., C.G.E., and D.G.W. revised manuscript; and P.M.K. wrote the paper.

The authors declare no competing interest.

This article is a PNAS Direct Submission.

[1]To whom correspondence may be addressed. Email: pkowale@uwo.ca.

This article contains supporting information online at https://www.pnas.org/lookup/suppl/doi:10.1073/pnas.2303119121/-/DCSupplemental.

Published February 13, 2024.

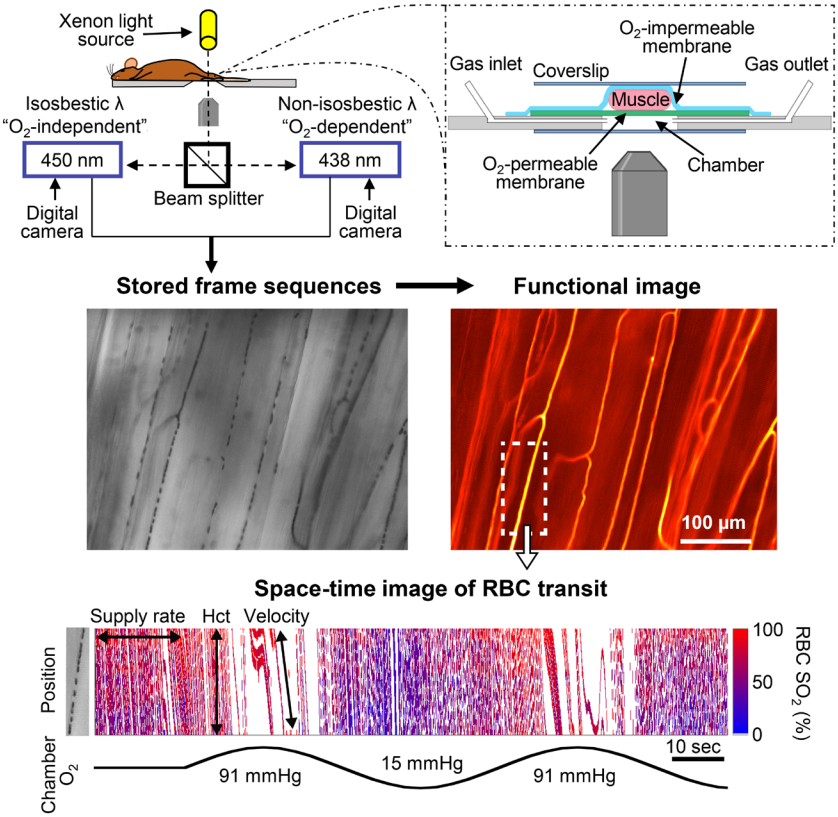

Fig. 1. Stage setup for dual-wavelength intravital microscopy and image analysis. Mice are positioned on a custom stage insert with a gas-exchange chamber, and the isolated EDL muscle is placed on an O_2-permeable membrane, covered with O_2-impermeable plastic wrap, and gently compressed with a coverslip. Warmed gas (N, CO_2, and O_2) is infused through the chamber, and O_2 levels in the chamber are tightly controlled at the surface of the muscle. Light transmitted through the muscle is split between two cameras and captured at two wavelengths that allow for calculation of RBC SO_2 based on spectral properties of fully oxygenated and deoxygenated hemoglobin. Functional images showing the passage of RBCs through capillaries are derived from the captured frame sequences, and space-time images are created for capillary segments showing RBC transit as tracts color-coded for SO_2. RBC dynamics are calculated from the space-time images. The RBC supply rate in the space-time image decreases when chamber O_2 levels are elevated and increases when chamber O_2 is lowered. Hct; hematocrit.

that O_2 responses are generated in capillaries and require Cx40-mediated conduction to arterioles to elicit RBC flow responses. Counter to the classical metabolic hypothesis and in line with the microcirculation acting as an O_2 sensor, genetic deletion of endothelial $K_{IR}2.1$, the molecular target of extracellular K^+, had no impact on responses to O_2. Together, these decisive and unique findings advance our mechanistic understanding of O_2 demand–supply coupling.

Results

Tissue PO_2 Simulations Are Not Consistent with Hypoxia. Tissue PO_2 at the muscle/chamber boundary was modeled as a multivessel arrangement with 72 uniformly spaced capillaries in an arteriolar to venous orientation on a 100-µm-thick fluorosilicone acrylate membrane atop the gas chamber (Fig. 2). All tissue blocks were modeled at steady state and assigned an inlet SO_2 of 76.5%. The calculated average surface PO_2 values (at the interface with the fluorosilicone acrylate membrane) for the low O_2 challenge before and after a flow response occurs were 45.4 mmHg (53 mmHg chamber O_2 with baseline flow), 26.4 mmHg (15 mmHg chamber O_2 with baseline flow), and 30.4 mmHg (15 mmHg chamber O_2 with flow response). The minimum simulated tissue PO_2 were: 19.6, 11.3, and 16.9 mmHg (respectively). As expected, the models predict that with the 15 mmHg challenge, tissue PO_2 does not fall below 10 mmHg, as estimated for tissue hypoxia (15–17); this argues against hypoxia-driven responses in our gas-exchange chamber experiments.

The calculated average surface PO_2 values during the 0% O_2 challenge were 18.0 mmHg without a flow response and 27.9 mmHg with a flow response. The minimum tissue PO_2 values were 0.3 and 14.7 mmHg, respectively. For the 0% O_2 challenge with no flow response, only a small region (0.2% of the domain) had local $PO_2 < 1$ mmHg due to the asymmetry of the capillary array and the no-flux boundary conditions used in the simulation.

***Cx40*$^{-/-}$ Mice Exhibit Lower RBC SO_2 but Normal Microhemodynamics.** Electrical coupling between ECs as well as smooth muscle cells (SMCs) is enabled by gap junctions composed of connexins. This connectivity is expected to be integral to the regulatory system ensuring proper O_2 distribution in tissues. To determine whether *Cx40*$^{-/-}$ animals have normal capillary hemodynamics, the exteriorized muscle was placed on a glass coverslip on a stage insert and covered with O_2-impermeable membrane so that the microcirculation was the only source of O_2 in the tissue. Capillary RBC velocity, hematocrit, and supply rate were similar between C57BL/6 control and *Cx40*$^{-/-}$ mice (Fig. 3 *A*–*C*). Intriguingly, however, capillary RBC SO_2 in *Cx40*$^{-/-}$ mice was significantly reduced compared to controls (Fig. 3*D*), possibly due to higher O_2 consumption or altered vascular network structure.

Cx40-Mediated Conduction Is Critical for O_2 Demand–Supply Coupling. It is not definitive whether skeletal muscle capillary RBC flow responses to local O_2 changes require Cx-mediated conducted signaling. Cx40 is one of the major Cx subunits that

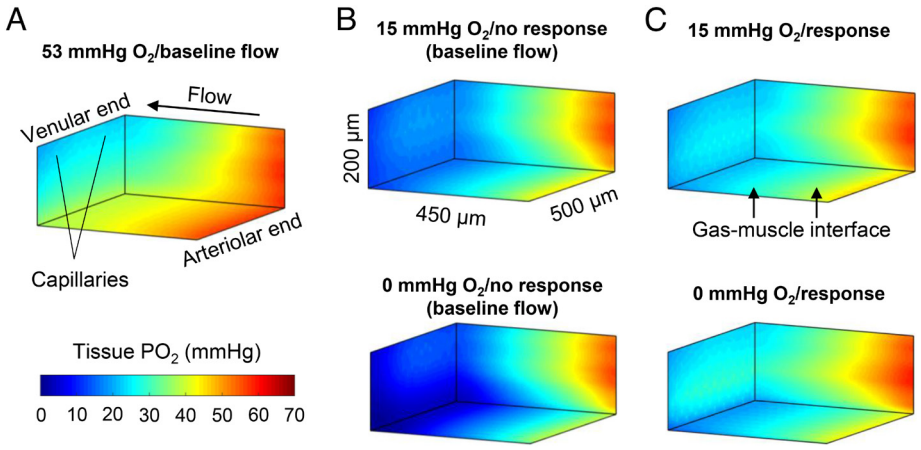

Fig. 2. Simulation of tissue PO_2 levels in skeletal muscle during a low O_2 challenge. 3D models of PO_2 distribution in the EDL muscle at the gas-muscle interface of the gas chamber are shown. The tissue PO_2 scenarios modeled are with gas chamber O_2 at 53 mmHg with baseline RBC flow levels (*A*), contrasted with 15 or 0 mmHg O_2 challenge without (*B*) and with (*C*) a capillary RBC flow response. The simulations predict that tissue does not become hypoxic during the O_2 challenges when there is an RBC flow response (*C*).

conduct electrical signals between ECs (18, 19). The lower RBC SO_2 in *Cx40*$^{-/-}$ mice led us to examine capillary flow responses to O_2 changes at the surface of the muscle. Decreased PO_2 can trigger different capillary RBC flow responses—increased RBC velocity, increased hematocrit, or both—adding up to an increased RBC supply rate. To probe the O_2 regulatory system, the EDL was placed on an O_2-permeable membrane of a custom stage gas chamber with a gas mixture flowing at 1 L/min with 53 mmHg O_2. Of note, 53 mmHg O_2 was chosen for baseline flow recordings because capillary RBC supply rates at this O_2 concentration match RBC supply rates in the muscle resting on a glass coverslip instead of the gas chamber in C57BL/6 mice (RBC supply rate in the muscle on a coverslip is 13.9 (8.9) RBC/s while on the gas chamber with 53 mmHg O_2 it is 13.5 (12.5) RBC/s). After the baseline recording, the chamber O_2 was lowered to 15 mmHg. Control EDL microcirculation responded with increased RBC velocity and increased capillary hematocrit, culminating in a significantly increased RBC supply rate (Fig. 4 *A* and *C* and Movie S1). When chamber O_2 was returned to 53 mmHg, the supply rate decreased to approximate baseline flow, suggesting the presence of a dynamic system that fine-tunes RBC supply to the local O_2 environment. *Cx40*$^{-/-}$ mice, on the other hand, failed to adequately adjust RBC flow in response to a sustained low O_2 challenge (Fig. 4 *B* and *C*). Surprisingly, the knockout mice did not exhibit a significant rise in RBC flow even when the 15 mmHg O_2 challenge was applied over 7 min (*SI Appendix*, Fig. S2). To further probe the O_2 demand–supply decoupling with global Cx40 deletion, we pushed the system by lowering chamber O_2 to 0 mmHg. Expectedly, control animals had a robust hemodynamic response to the 0% O_2 challenge while the *Cx40*$^{-/-}$ mice did not (Fig. 4*D*). When data were presented as individual values per capillary, it became apparent that upon a 0 mmHg O_2 challenge, the *Cx40*$^{-/-}$ microvasculature attempted to respond with a slight hematocrit increase (Fig. 4*D*). Due to the severely diminished RBC flow response with Cx40 deletion, RBC SO_2 levels trended lower during the O_2 challenges in *Cx40*$^{-/-}$ capillaries, but the difference was not statistically significant compared to controls (*SI Appendix*, Fig. S3).

To assess SMC function in *Cx40*$^{-/-}$ mice, arterial capacity to dilate and constrict was verified with capillary RBC flow measurements at baseline and after topical application of an SMC-dependent vasodilator (sodium nitroprusside), a constrictor (phenylephrine HCl), followed by an endothelium-dependent dilator (acetylcholine). The microcirculation of the *Cx40*$^{-/-}$ mice responded to these agonists (*SI Appendix*, Fig. S4).

To examine how rapid and tightly coupled hemodynamic responses are when O_2 levels are varied at the surface of the muscle, chamber O_2 was oscillated in a sinusoidal fashion between 15 and 91 mmHg O_2. Second-by-second traces of the RBC supply rate in control animals oscillated in concert with the chamber O_2 levels (*SI Appendix*, Fig. S5*A*). Again, *Cx40*$^{-/-}$ mice did not respond to rapid (1-min) sinusoidal O_2 oscillation as the control animals (*SI Appendix*, Fig. S5*B*). Thus, the rapid and graded microcirculatory responses to O_2 are diminished in the absence of Cx40-mediated conduction. Taken together, it appears that,

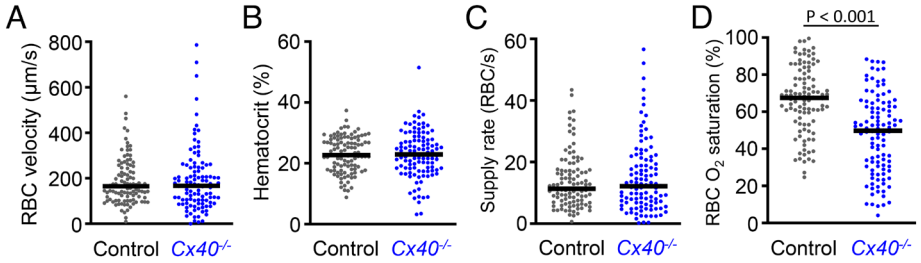

Fig. 3. *Cx40*$^{-/-}$ mice have normal capillary RBC dynamics but significantly lower RBC SO_2. To assess resting capillary RBC dynamics, the EDL muscle was placed on a glass coverslip and covered with O_2-impermeable membrane so that microcirculation was the only source of O_2. *Cx40*$^{-/-}$ mice have normal capillary RBC velocity (*A*), hematocrit (*B*), and supply rate (*C*) but significantly lower RBC SO_2 (*D*) compared to control. The distribution of data is shown as median and individual values from 105 capillaries in the C57BL/6 control group of 6 mice and 108 capillaries in the knockout group of 8 mice. Statistical differences in RBC velocity and supply rates between control and knockout mice were assessed using the Mann–Whitney test; differences in capillary hematocrit and RBC SO_2 were assessed using the unpaired *t* test.

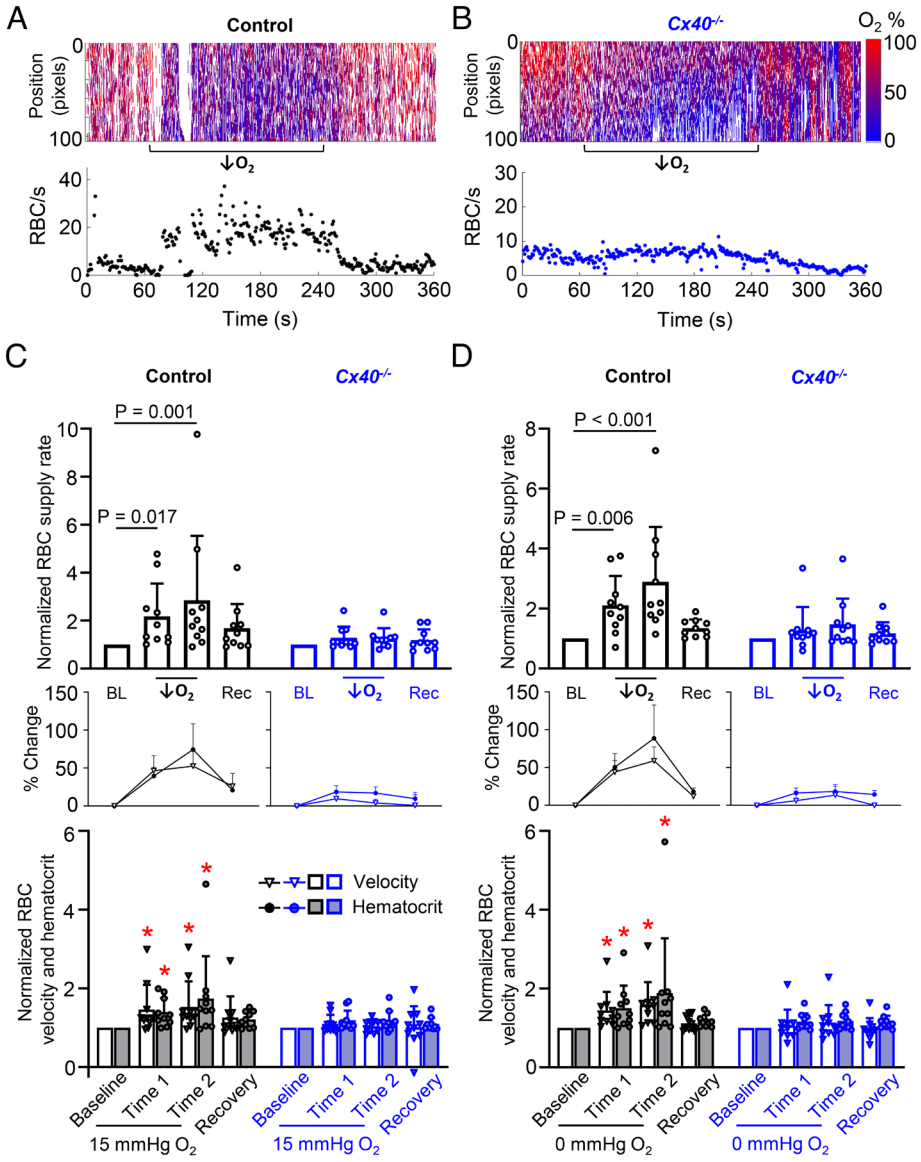

Fig. 4. Microvascular responses to decreased O_2 at the skeletal muscle surface are severely diminished in *Cx40*$^{-/-}$ mice. After baseline measurement of capillary hemodynamics, the skeletal muscle surface was exposed to decreased O_2 in the gas chamber, and RBC flow responses were quantified. Representative space-time images and corresponding capillary RBC supply rate traces during a low O_2 challenge are shown for a representative capillary from a control (*A*) and a *Cx40*$^{-/-}$ mouse (*B*). Summary data for RBC supply rate, velocity, and hematocrit in capillaries from control and *Cx40*$^{-/-}$ mice during 15 (*C*) and 0 mmHg (*D*) O_2 challenge. Values were normalized to baseline and reported as mean (SD) with $n = 10$ mice in each group. These data are based on 61 capillaries in the control group and 68 capillaries in the knockout group. Repeated-measures one-way ANOVA with Šídák's multiple comparisons test was used for parametric data, and the Friedman test (repeated measures) with Dunn's multiple comparisons test was used for nonparametric data, $^*P < 0.05$ compared with baseline. For illustrative purposes, line graph *Insets* show % change in normalized RBC velocity vs. hematocrit across individual capillaries in each group. BL; baseline, Rec; recovery.

despite normal RBC flow in *Cx40*$^{-/-}$ capillaries at rest (Fig. 3), RBC flow deficiencies emerge when O_2 demand changes (Fig. 4 and *SI Appendix*, Fig. S5).

Cx37 and Cx40 Are Abundantly Expressed in the Capillary Endothelium. To characterize the connexin subunit composition in the capillary endothelium of the EDL, immunolabeling approaches were used on ex vivo muscle samples targeting the major EC subtypes Cx37 and 40. Both were expressed in the capillaries of C57BL/6 control animals (Fig. 5 *A*–*D*). Cx37 was localized to capillaries in *Cx40*$^{-/-}$ mice as well (Fig. 5 *E* and *F*). As expected, anti-Cx40 did not label capillaries in *Cx40*$^{-/-}$ muscles (Fig. 5 *G* and *H*). The observed Cx40 expression in EDL capillaries is in line with the hypothesis that diminished RBC flow responses to low O_2 in *Cx40*$^{-/-}$ muscles are due to limited conducted signaling from the capillary endothelium.

O_2 and Not Hypoxia Drive RBC Flow Responses. As inferred from the tissue PO_2 simulations (Fig. 2), our experimental setup is not designed to induce tissue hypoxia, and the 15 mmHg O_2 challenge is above the estimated 2 to 3 mmHg limit for mitochondrial O_2 consumption (16, 20). This means the observed capillary RBC flow responses do not need hypoxic conditions to become triggered. To further drive this point, the O_2 challenges were inverted by increasing the chamber O_2 level from a baseline of 53 to 91 or 152 mmHg for 3 min and sustained capillary RBC flow responses in C57BL/6 control mice were observed. The increased PO_2 generally reduced RBC flow through capillary networks in control mice (Fig. 6 *A*–*D*) with shut-off or even slightly reversed RBC flow in a small portion of capillaries. This RBC flow decrease was more profound with 152 mmHg (Fig. 6*C*). Thus, capillary RBC supply rates are proportionally and directionally coupled to O_2; lower O_2 increases RBC flow and higher O_2 decreases RBC

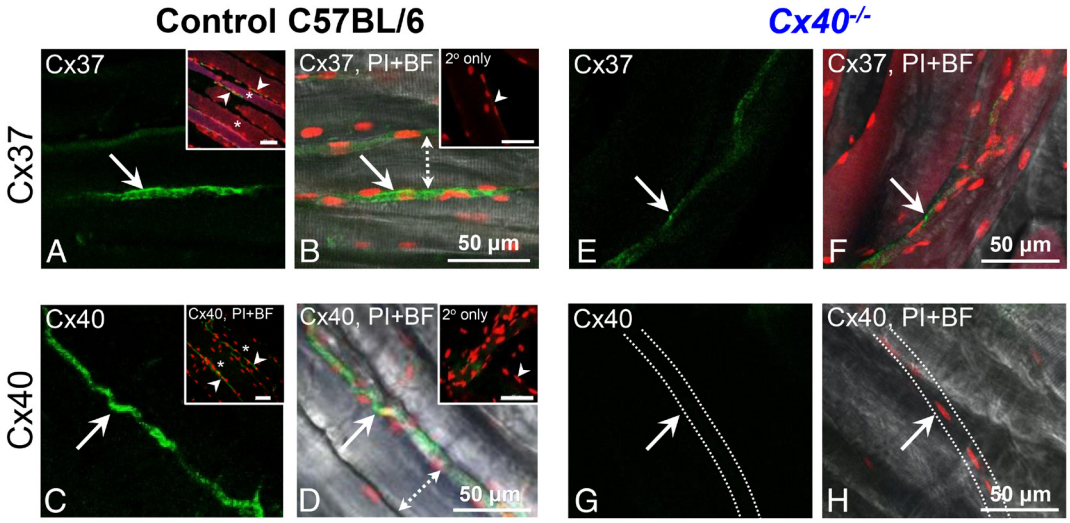

Fig. 5. Cx37 and 40 distribution (green) in mouse EDL (skeletal muscle) capillaries from control C57BL/6 (*A–D*) and *Cx40*$^{-/-}$ (*E–H*) mice. Connexins 37 and 40 in the EDL capillary endothelium of control (*A* and *B*; *C* and *D*, respectively) and Cx37 (*E–F*), but not Cx40 (*G* and *H*), in *Cx40*$^{-/-}$ mice. Propidium iodide (PI; red) nuclei label indicates cell and vessel patency. Low magnification *Insets* (*A* and *C*) show capillary (arrowhead) and skeletal muscle fiber (*) long axis approximate parallel alignment, with capillaries running primarily along muscle fiber edges (see also *B* and *D* with skeletal muscle cross-section axis in the bright field; BF, vertical double arrow). Secondary antibody control (*B* and *D*, *Inset*, at the capillary endothelium focal plane, indicated by the PI label and arrowhead). The dashed line (*G* and *H*) indicates approximate capillary edge in *Cx40*$^{-/-}$ EDL. Arrows (*A–H*) indicate the same location in the respective panels. *n* = 6 control and 2 *Cx40*$^{-/-}$ mice. (Scale bar in *Insets*, 50 µm.)

flow. In *Cx40*$^{-/-}$ mice, 91 mmHg O_2 challenge reduced flow, but not to a statistically significant degree; 152 mmHg O_2 challenge, however, significantly reduced RBC flow in the *Cx40*$^{-/-}$ capillaries, indicating that a stronger albeit unphysiological stimulus triggers appreciable flow responses in these mice (Fig. 6 *E* and *F*).

Endothelial *$K_{IR}2.1^{-/-}$* Mice Have Normal Capillary RBC Dynamics, and Extracellular K^+ Does Not Trigger RBC Flow Responses to O_2. Under the branch of metabolic hypotheses, one of the mechanisms of blood flow regulation involves the interstitial accumulation of K^+, a potent vasodilatory stimulus acting through endothelial $K_{IR}2.1$ channels, which amplify endothelium-dependent dilation (13, 14) and mediate functional hyperemia, notably in the brain (2, 12, 21). We tested this mechanism in O_2 regulation in skeletal muscle by employing EC *$K_{IR}2.1^{-/-}$* mice. Whether these mice have normal capillary hemodynamics was determined by measuring microcirculatory flow with the EDL positioned on a glass coverslip. Capillary RBC supply rate, velocity, hematocrit, and RBC SO_2 were similar between floxed control and EC *$K_{IR}2.1^{-/-}$* mice at rest (Fig. 7). The O_2 regulatory system was tested next. Mice deficient in EC $K_{IR}2.1$ had normal capillary RBC flow responses to a sustained 15 and 0 mmHg O_2 challenge (Fig. 8). Thus, even with the 0-mmHg challenge, it does not appear that extracellular K^+ signaling plays a role. Also, EC *$K_{IR}2.1^{-/-}$* mice responded to O_2 oscillations similarly to floxed controls (*SI Appendix*, Fig. S6). Evidently, $K_{IR}2.1$ channels do not mediate microvascular responses to O_2 changes in skeletal muscle capillaries. This implies that elevated interstitial K^+, which activates EC $K_{IR}2.1$ to trigger hyperpolarization and vasodilation, is not a driver of these responses.

O_2 Responses Are Triggered in Capillaries without Microvascular Divergence among Control and *$K_{IR}2.1^{-/-}$* Mice. It could be argued that EC *$K_{IR}2.1^{-/-}$* mice in the present study exhibited normal responses to low O_2 because the stimulus applied with the full O_2-permeable window encompassed several bundles of surface capillaries across one side of the muscle, masking any deficits. Thus, the size of the window was reduced to 400 by 200 µm (Fig. 9*A*) to target a smaller number of capillaries, likely belonging to one bundle. Specifically, this microwindow fits approximately 10 surface capillaries and was positioned over their venular end. Lowering O_2 from 53 to 15 mmHg at the microwindow elicited an increased RBC supply rate in capillaries of C57BL/6 control animals (Fig. 9 *B* and *C*), consistent with the idea that conducted vasodilatory responses arise at the level of the capillary (9, 22). Interestingly, the increased supply rate was due to significantly increased hematocrit in the capillaries and not velocity (Fig. 9*D*). Thus, stimulating a smaller area of the muscle triggers a flow response dominated by hematocrit changes. This localized stimulus may adjust tone in upstream arteriolar bifurcations to change hematocrit but may not be sufficient to change velocity. We next confirmed that this capillary response is not abrogated nor blunted in EC *$K_{IR}2.1^{-/-}$* muscles (Fig. 9*C*), which had significantly increased hematocrit as well in response to the localized low O_2 stimulus (Fig. 9*D*). This confirms that O_2 regulatory responses are intact in the absence of EC $K_{IR}2.1$ despite a smaller stimulus.

Computational Modeling of RBC Distribution for Diverging Arteriolar Bifurcations. Bifurcations at terminal arterioles were modeled using measured diameters from vascular networks (*SI Appendix*, Fig. S7). For a given set of parent (D_0) and daughter ($D_1 > D_2$) diameters, assuming an initial value of hematocrit (H_2) = 0.2 sets the initial blood flow fraction (q_2). Changes in H_2 and RBC flow fraction (f_2) in the smaller daughter branch were calculated based on a 10% increase in q_2. The results of the simulations based on different vessel diameter scenarios (*SI Appendix*, Fig. S8) show that having a capillary-sized parent vessel leads to relatively large increases in H_2 and f_2, consistent with the observed hematocrit-dominated responses when a single capillary module is stimulated with low O_2 using the microwindow on the gas-exchange chamber.

Discussion

Microvascular networks are tasked with swiftly and proportionally meeting the O_2 demands of tissues. How this mechanistically occurs remains an open question, with the present study pursuing the idea that O_2 changes in capillaries generate signals that effectively control tone in upstream resistors. In this regard, we used a

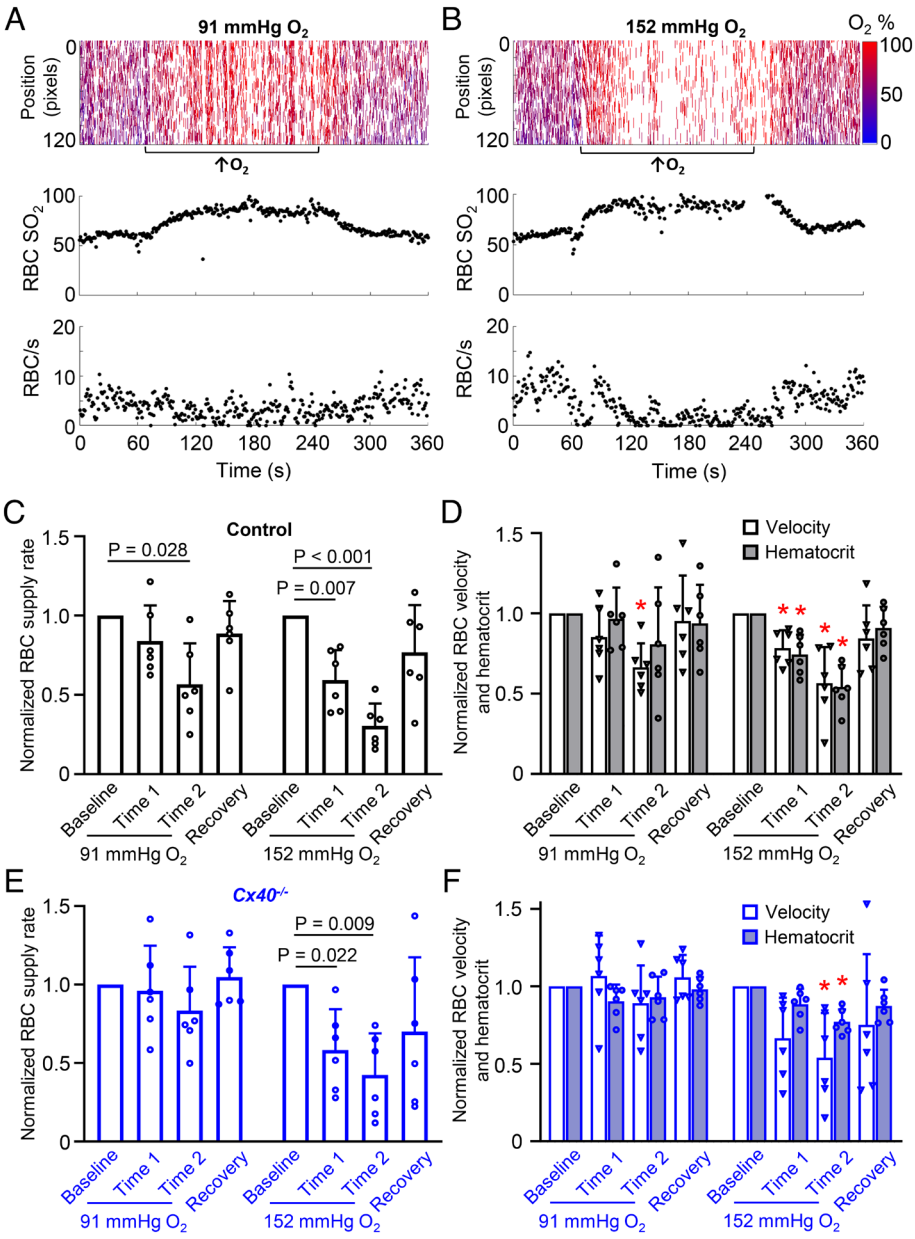

Fig. 6. Capillary RBC flow responses to high O_2 challenge. The skeletal muscle surface was exposed to increased O_2 in the gas chamber after baseline flow recording and RBC flow responses were quantified. Representative space-time images with corresponding RBC O_2 saturation and supply rate traces are from the same capillary from skeletal muscle of a C57BL/6 mouse recorded during a high O_2 [91 (*A*) or 152 mmHg (*B*)] challenge. Summary data for capillary RBC supply rate (*C*), velocity and hematocrit (*D*) during the high O_2 challenge from C57BL/6 mice, with corresponding graphs from *Cx40*$^{-/-}$ mice (*E* and *F*). Values were normalized to baseline, reported as mean (SD) with $n = 6$ mice (based on 62 and 59 capillary measurements from control and knockouts, respectively) and determined to be normally distributed. Repeated-measures one-way ANOVA with Šídák's multiple comparisons test was used to determine significant differences from baseline (*$P < 0.05$).

unique approach to manipulate RBC SO_2 and tissue PO_2 to drive changes in capillary RBC flow in control and genetic deletion mice to determine the requirement for Cx-mediated vascular conduction as well as the relevance of extracellular K^+ signaling in O_2 demand–supply coupling. Results indicate that Cx40-mediated conduction is critical for capillary signaling to the upstream arteriolar network to match RBC flow to O_2 needs. Present data also challenge aspects of the metabolic hypothesis by finding no role for hypoxia nor activation of EC $K_{IR}2.1$ by extracellular K^+, refocusing the current paradigm of O_2 regulation.

O_2 as the Stimulus. This study shows that microcirculatory responses are directional and proportional to the magnitude of the O_2 stimulus. This was noted as RBC supply rate increased in response to dropping chamber O_2 and decreased when chamber O_2 was raised (Fig. 4 and *SI Appendix*, Figs. S5 and S6), and was also affected by the magnitude of the stimulus, as evidenced by use of the microwindow (Fig. 9). The reduction of capillary RBC flow by elevated O_2 at the muscle surface is consistent with O_2 rather than hypoxia being the stimulus driving blood flow responses. This idea aligns with computational simulations (Fig. 2), which predict that low O_2 challenges, over a 3-min perturbation, do not reduce surface muscle PO_2 sufficiently to compromise mitochondrial respiration (20). Notably, O_2 as the stimulus (as opposed to hypoxia) would allow the system to adjust RBC flow before reaching the hypoxic state; a state that, after all, blood flow regulation aims to prevent.

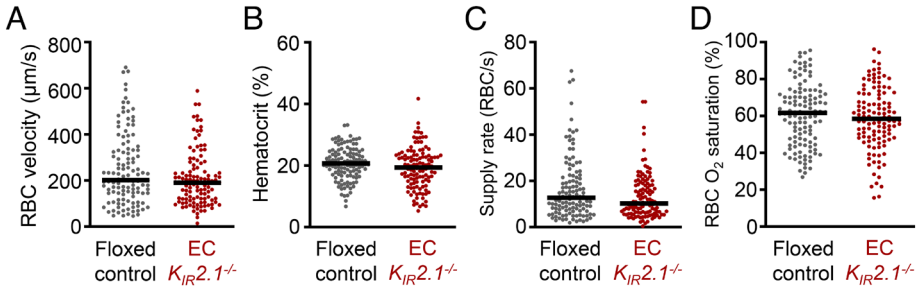

Fig. 7. EC $K_{IR}2.1^{-/-}$ mice have normal capillary RBC dynamics and RBC SO_2. To assess resting capillary RBC dynamics, the EDL muscle was placed on a glass coverslip and covered with O_2-impermeable membrane so that microcirculation was the only source of O_2. EC $K_{IR}2.1^{-/-}$ mice have similar resting capillary RBC velocity (*A*), hematocrit (*B*), and supply rate (*C*), and RBC SO_2 (*D*) compared to floxed control mice. The distribution of data is shown as median and individual values from 120 capillaries in the floxed control group of 6 mice and 116 capillaries in the knockout group of 7 mice. Significant differences (defined as $P < 0.05$) in RBC velocity and supply rates between floxed control and knockout mice were assessed using the Mann–Whitney test; differences in capillary hematocrit and RBC SO_2 were assessed using the unpaired *t* test.

Capillaries as the Site of O_2 Sensing. Given the regular and intimate location of capillaries along muscle fibers, it stands to reason capillaries are the site of O_2 sensing while arterioles are the site of RBC flow control (5, 23). Indeed, evidence exists that discrete application of vasoactive agents on capillaries evokes upstream arteriolar diameter changes and increased blood flow, a

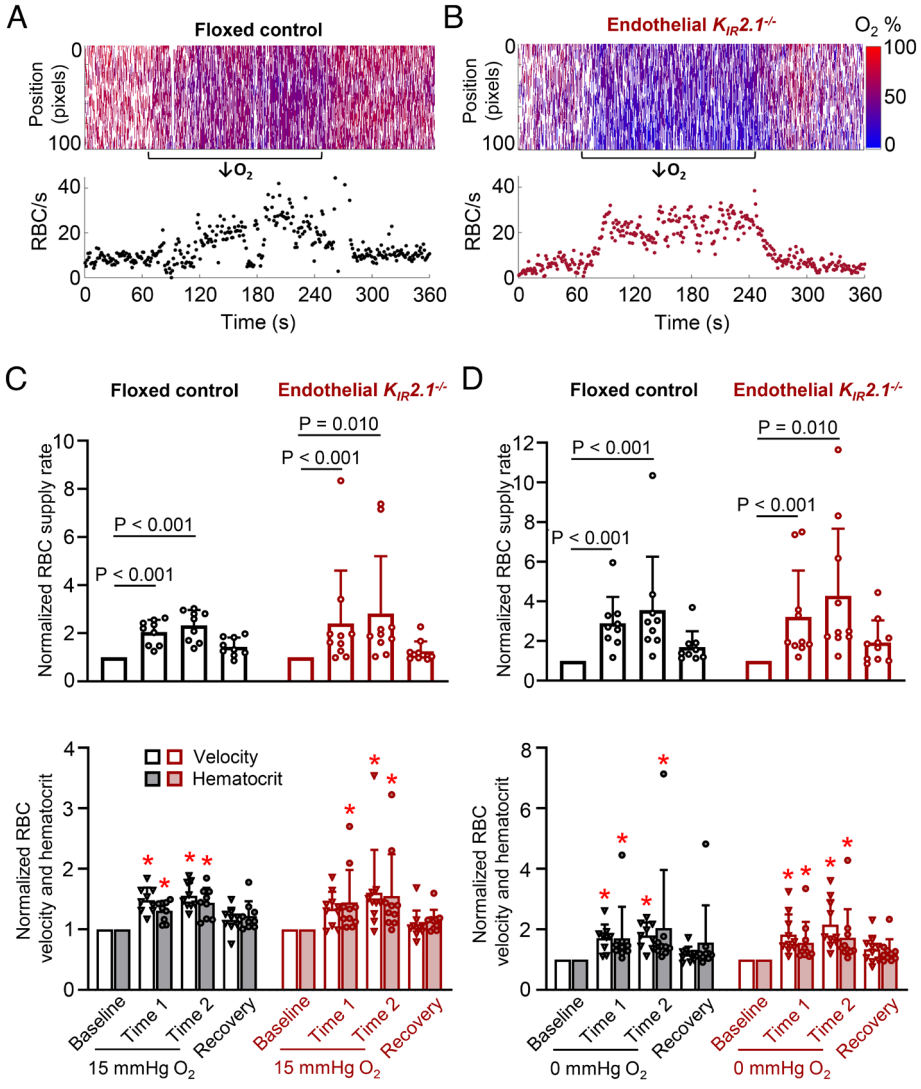

Fig. 8. Microvascular responses to decreased O_2 at the muscle surface are intact in endothelial $K_{IR}2.1^{-/-}$ mice. Representative space-time images and corresponding capillary RBC supply rate traces during a low O_2 challenge are shown for a control (*A*) and endothelial $K_{IR}2.1^{-/-}$ mouse (*B*). Summary data for RBC supply rate, velocity, and hematocrit in capillaries from control and knockout mice during 15 (*C*) and 0 mmHg (*D*) O_2 challenge. Values were normalized to baseline and reported as mean (SD) with $n = 9$ mice in the floxed group and $n = 10$ mice in the knockout group. These data are based on 83 capillaries in the control group and 78 capillaries in the knockout group. Repeated-measures one-way ANOVA with Šídák's multiple comparisons test was used for parametric data, and the Friedman test (repeated measures) with Dunn's multiple comparisons test was used for nonparametric data, *$P < 0.05$ compared with baseline.

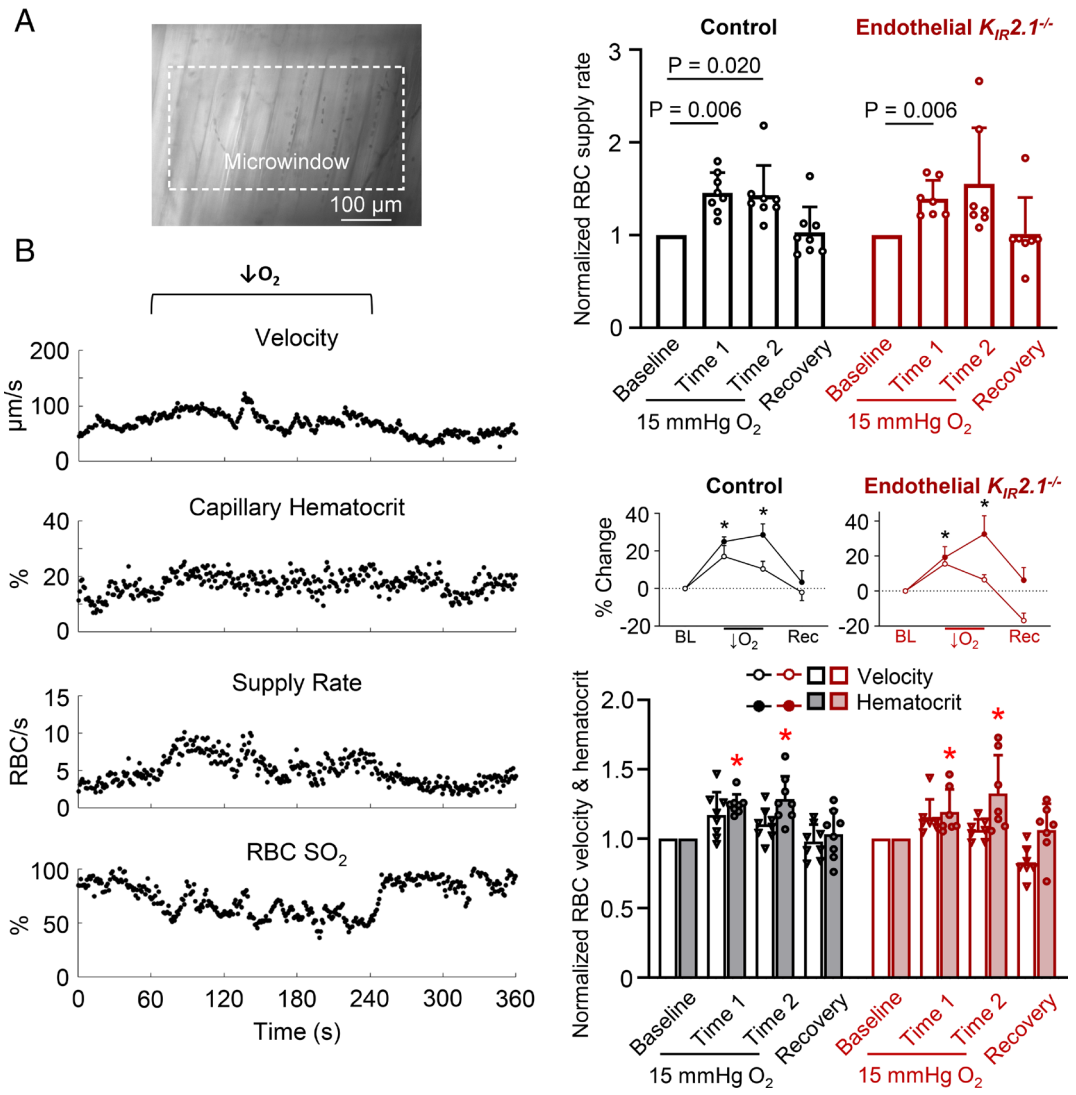

Fig. 9. Microhemodynamic responses to a localized O_2 stimulus are elicited in C57BL/6 control and endothelial $K_{IR}2.1^{-/-}$ EDL capillaries and are dominated by hematocrit changes. To stimulate a small number of capillaries near the surface, the muscles were positioned over a microwindow (*A*) of a specialized gas-exchange chamber. Traces of a representative hemodynamic response to 15 mmHg O_2 for a capillary (C57BL/6 mouse) are shown (*B*). Summary data for RBC supply rate (*C*), velocity and hematocrit (*D*) in capillaries from control and endothelial $K_{IR}2.1^{-/-}$ mice during 15 mmHg O_2 challenge. Values were normalized to baseline and reported as mean (SD) with $n = 10$ mice in each group. These data are based on 83 capillaries in the control group and 67 capillaries in the knockout group. Repeated-measures one-way ANOVA with Šídák's multiple comparisons test was used for parametric data, and the Friedman test (repeated measures) with Dunn's multiple comparisons test was used for nonparametric data, $*P < 0.05$ compared with baseline. For illustrative purposes, line graph *Insets* show % change in normalized RBC velocity vs. hematocrit in each group, highlighting the dominance of hematocrit changes in this localized response. BL; baseline, Rec; recovery.

process requiring EC-EC coupling via gap junctions (24, 25). To target the O_2 stimulus to a limited number of capillaries, the O_2 challenge was applied to a smaller volume of tissue by scaling the O_2-permeable window down to the micrometer range. Positioning this "microwindow" over a few capillaries at their venular end to apply a low O_2 challenge increased RBC flow through these capillaries, albeit with a lesser magnitude compared to the larger window that overlays many surface capillaries (Fig. 9 vs. Fig. 4). This finding is in accordance with observations that individual capillary units govern their own supply of RBCs to different tissue PO_2 levels (9, 22).

Cx40-Mediated Conduction Is Crucial for O_2 Demand–Supply Coupling. Intercellular communication is mediated by clusters of paired connexons known as gap junctions, each connexon being composed of 6 connexins in the membrane of adjacent cells. These gap junctions couple neighboring cells chemically and electrically, allowing cells to share small molecules <~1 kDa, such as current-generating ions and intracellular mediators including cAMP and IP_3 (26, 27). Electrophysiological approaches determined that coupling resistance is lower between ECs, intermediate between SMCs, and highest between EC and SMCs (28), which is proportional to gap junction density (29). Cx37, 40, and 43 dominate connexin expression at interendothelial junctions, Cx40 is one of the subunits present at myoendothelial junctions, and Cx43 and 45 predominate at SMC junctions (30, 31). The physical contact between vascular cells underlies the principle of the conducted response and explains how the endothelium drives smooth muscle hyperpolarization and vasodilation spanning more than 1 mm of vessel length.

Using immunofluorescence approaches, the expression of the key endothelial connexins, Cx37 and 40, was verified in skeletal muscle capillaries (Fig. 5). With Cx40 being a chief mediator of conducted vasodilation (32), microcirculatory dynamics in skeletal muscle of $Cx40^{-/-}$ mice were assessed (Fig. 3). Intriguingly, capillary RBC dynamics were normal in knockouts but RBC SO_2

was significantly reduced. Such findings suggest that *Cx40*$^{-/-}$ mice may have increased O_2 consumption without a sufficient increase in the RBC supply rate to maintain RBC SO_2, indicative of an ineffectual O_2 regulatory system.

The decreased RBC SO_2 levels prompted exploration of the O_2 regulatory system in these knockout mice using the gas-exchange platform to induce a sustained low O_2 step change in muscle tissue PO_2 (Fig. 4). When chamber O_2 was lowered to 15 mmHg, control animals exhibited an increased RBC supply rate, velocity, and hematocrit, while these microhemodynamic responses were diminished in *Cx40*$^{-/-}$ mice. Pushing the system further by dropping the chamber O_2 level to 0 mmHg elicited a strong RBC flow response in control muscles while responses in the *Cx40*$^{-/-}$ microvasculature were inadequate and limited to a slight elevation in hematocrit. Likewise, capillary flow responses to oscillatory tissue PO_2 changes were markedly diminished in *Cx40*$^{-/-}$ mice (*SI Appendix*, Fig. S5). However, a high O_2 challenge at 152 mmHg significantly reduced the RBC supply rate in *Cx40*$^{-/-}$ mice (Fig. 6), indicating that the genetic deletion does not abolish conduction but merely diminishes it. Taken together, these findings demonstrate that Cx-mediated conduction is central to O_2 demand–supply coupling and can be explained by capillary endothelial hyperpolarization spreading to upstream arteriolar endothelium and SMCs, resulting in vasodilation and increased capillary RBC supply rate.

Notably, global *Cx40*$^{-/-}$ mice have an increased incidence of cardiac malformations, albeit in a heterogeneous manner (33), and were reported to be hypertensive (34) due to increased renin secretion (35). However, the effects of this phenotype do not appear to alter microvascular RBC flow in the EDL, as shown by the comparable capillary hemodynamics between the control and *Cx40*$^{-/-}$ mice in the muscle at rest (Fig. 3). Nevertheless, a limitation of our study is that we were unable to obtain a conditional EC-specific *Cx40*$^{-/-}$ mouse line to further confirm our findings and conclusion. This mouse strain would further isolate observations from other mural cells. In this regard, some reports argue that vascular smooth muscle itself senses and responds to O_2 changes (36, 37). However, such works tend to use isolated larger-bore vessels, which may not translate to smaller arteries or arterioles, the latter contributing substantially to vascular resistance and blood flow control. Furthermore, no detectable O_2 sensitivity in SMCs was reported (38–42). Considering the contradictory literature, it could be argued that *Cx40*$^{-/-}$ mice have dysfunctional vascular SMCs. Therefore, we verified whether arteries of *Cx40*$^{-/-}$ mice respond to basic dilator/constrictor agonists in vivo, including the SMC-dependent agonist sodium nitroprusside, and have shown that the microcirculation of *Cx40*$^{-/-}$ mice responds accordingly (*SI Appendix*, Fig. S4). Thus, it appears Cx-mediated EC-EC coupling is limited in the Cx40 knockout as opposed to vascular SMC dysfunction.

Two Types of RBC Flow Responses, Velocity and Hematocrit, Are Tied to the Magnitude of the O_2 Stimulus. The microwindow experiments indicate that capillary supply rate responses are graded according to the tissue area stimulated. The magnitude of the RBC supply rate increase in capillaries exposed to 15 mmHg O_2 was smaller when the low O_2 stimulus was scaled down to a small number of capillaries [microwindow (Fig. 9) vs. full window (Fig. 4)]. Interestingly, the increased supply rate with the smaller window was mainly a product of increased hematocrit as opposed to RBC velocity, in line with observations in rat EDL (9). This finding emphasizes that RBC flow responses are more than a change in blood flow rate; they reflect a redistribution of RBCs vs. plasma, which is inevitably tied to the magnitude of the stimulus, EC-EC coupling, conduction distance, and structure of the arterial network (*SI Appendix*, Fig. S9). Electrical modeling of the vasculature as well as experimental evidence from mesenteric resistance arteries showed that conduction is endothelium-driven as EC disruption limits conduction past that point (43). Furthermore, modeling approaches indicate that conduction decay increases with longer vessels and branch points, the impact of the latter diminished if both daughter vessels are stimulated. In this model, increasing EC-EC coupling resistance impacted vasomotor and blood flow responses (43).

Considering the components of blood flow (RBC supply rate and plasma flow), our theoretical results (*SI Appendix*, Fig. S8) show that having relatively small parent vessels (diameter of ~6 vs. ~15 μm) leads to greater relative changes in hematocrit in a capillary module, which was observed experimentally with the microwindow (Fig. 9). However, the model predicts changes in hematocrit and RBC supply that are slightly smaller than those that were measured; this may be because a single bifurcation was considered in this theoretical model, while there are likely some RBC redistribution effects occurring at several arterial branch levels in the EDL muscle positioned on the microwindow. With the full chamber window, one would predict that the signal conducts further upstream, altering flow distribution at bifurcations with larger diameters which favors changes in velocity over hematocrit.

Extracellular K^+ Does Not Trigger Microhemodynamic Responses to O_2 in the Skeletal Muscle. Extracellular K^+ is a potent vasodilator implicated in O_2 demand–supply coupling. In the brain, it was shown that accumulation of K^+ in the discrete extracellular space activates $K_{IR}2.1$ channels in the capillary endothelium, generating a hyperpolarization that conducts along coupled ECs to arterioles, enabling functional hyperemia (12). Thus, $K_{IR}2.1$ channels position capillary ECs as K^+ sensors that initiate conducted vasodilation. Whether this $K_{IR}2.1$-mediated mechanism enables tissue PO_2 to drive capillary RBC delivery in skeletal muscle remains unclear. Thus, RBC flow responses to low O_2 in EC-specific *$K_{IR}2.1$*$^{-/-}$ mice were probed. Microhemodynamics in the EDL were assessed, revealing that RBC supply rates, velocity and hematocrit, as well as RBC SO_2 are normal in these knockout mice (Fig. 7). It was further demonstrated that capillary flow responses in EC *$K_{IR}2.1$*$^{-/-}$ mice were intact, irrespective of the O_2 challenge [step change (Fig. 8), or oscillation (*SI Appendix*, Fig. S6)]. It could be reasoned that the full O_2-permeable window allowed stimulation of enough capillary modules to generate a response in these knockout mice, masking any deficiencies. Thus, in a confirmatory experiment, the number of capillaries exposed to low O_2 was reduced using a microwindow, showing comparable RBC flow responses in the knockouts and controls, which were dominated by hematocrit changes (Fig. 9). Thus, microhemodynamic responses evoked by decreased O_2 are independent of endothelial $K_{IR}2.1$ and extracellular K^+ in healthy resting skeletal muscle. However, these results do not contest a role for extracellular K^+ in heavy exercise or in pathologic/hypoxic conditions.

Proposed Mechanism. The array of cell types theorized to be O_2 sensors spans vascular cells (ECs or SMCs), extravascular cells (parenchyma/mitochondria, nerves or perivascular mast cells), and RBCs (7). As our data are in line with the idea that RBC flow responses are initiated at the level of the capillary, we consider that the RBC itself may act as the sensor. Specifically, hemoglobin desaturation may trigger capillary hyperpolarization through ATP release from RBCs via pannexin-1, which activates endothelial purinergic receptors (5, 44–46). This, in turn, results in activation of hyperpolarizing channels in the capillary endothelium and Cx40-mediated conducted signaling from capillary ECs to arteriolar SMCs (*SI Appendix*, Fig. S10). Further approaches will be required to fully clarify this pathway.

Pathophysiological Significance: Microvascular Dysfunction in Sepsis. The present findings underpin a key role for conduction in O_2 signaling, with Cx40 deletion leading to diminished capillary responses to decreased tissue O_2 tension. Such deficits are believed to underlie pathophysiological processes in diseases such as sepsis, where microvascular dysfunction is an early event (47) leading to abnormal microvascular flow patterns (48). Indeed, vascular communication is impaired in early sepsis, evidenced by diminished conducted responses in mouse skeletal muscle vasculature (49, 50). Specifically, sepsis limited conducted hyperpolarization along the capillary endothelium to the upstream arteriole (51). Thus, the dysfunctional microvasculature in sepsis exhibits breakdown of interendothelial electrical coupling. Interestingly, this reduced coupling was found to be associated with lipopolysaccharide-induced dephosphorylation of Cx40 (52).

Summary. This work examined O_2-driven microhemodynamic responses in healthy skeletal muscle at rest. The present data are in line with 1) capillaries as the site where O_2 requirements are sensed, and RBC flow responses are initiated; 2) Cx40-mediated electrical communication between capillaries and upstream arterioles. This work challenges the idea that hypoxia triggers microcirculatory responses in healthy muscle and is inconsistent with the accumulation of extracellular K^+ and activation of endothelial $K_{IR}2.1$ channels as the driving event. These findings refocus the O_2 demand–supply coupling paradigm in skeletal muscle to O_2 as the stimulus, microcirculation as the sensor, and capillaries as the site of initiation of conducted hyperpolarization, ultimately leading to arteriolar vasodilation and increased delivery of O_2-rich RBCs.

Materials and Methods

Animals. Animal protocols met regulations set by the Canadian Council of Animal Care and were approved by the University of Western Ontario Animal Care Committee (Protocol #2018-107 and 2016-006). Colonies of EC $K_{IR}2.1^{-/-}$ mice [strain B6.Cg-Kcnj2^{tm1Swz} tg(Tek-cre)1Ywa] (14), floxed $K_{IR}2.1$ control mice (strain B6.Cg-Kcnj2^{tm1Swz}) (14, 53), and $Cx40^{-/-}$ mice (strain B6.129S4-Gja5^{tm1Paul}; available from The Jackson Laboratory (strain 025697); Bar Harbor, ME, USA) were maintained at the University of Western Ontario. C57BL/6J male mice (strain 000664) were obtained from The Jackson Laboratory. The animals were communally housed under constant temperature and humidity with a 12-h light/dark cycle and free access to food and water. At the time of use, the male mice weighed 25 g to 32 g and were approximately 16 wk old.

Surgical Preparation. Mice were anesthetized with an intraperitoneal (IP) injection of urethane (962 mg/kg; Sigma-Aldrich, Oakville, ON, Canada) and α-chloralose (72 mg/kg; Sigma-Aldrich). The absence of corneal and pedal reflexes was monitored, and maintenance doses were administered IP as needed. Animals were given 0.4 mL subcutaneous fluids to compensate for evaporative loss during surgery. An incision was made in the skin over the anterolateral aspect of the right hindlimb. Fascia was split between the tibialis cranialis and gastrocnemius lateralis. The right EDL was isolated from surrounding muscles, and its tendon was secured with a silk suture (5–0) and severed distal to the ligature.

For O_2-challenge experiments, the animals were positioned on a custom stage insert with a gas-exchange chamber containing a large O_2-permeable window (herein termed "full window"). The suture on the EDL tendon was secured to the stage, keeping the muscle at its in situ length with one of its sides directly over the O_2-permeable membrane (fluorosilicone acrylate, 100 μm thick; Paragon Vision Sciences, Mesa, AZ, USA) of the window (Fig. 1). Thus, this window exposed one side of the isolated muscle to flowing O_2. The EDL was bathed in Plasma-Lyte A (37 °C, pH 7.4, Na 140 mmol/L, Cl 98 mmol/L, K 5 mmol/L, Mg 1.5 mmol/L, acetate 27 mmol/L, gluconate 23 mmol/L, osmolarity 294 mOsmol/L; Baxter Corporation, Mississauga, ON, Canada), isolated from the environment with an O_2-impermeable polyvinylidene chloride film (Saran Wrap; Dow Chemical Company, Midland, MI, USA), and gently compressed with a glass coverslip. The EDL muscle microcirculation was stabilized with warmed (37 °C) 5% O_2, 5% CO_2 and balanced N_2 mixture in the chamber for >20 min on the microscope stage before recording. The mice respired supplemental 34% O_2 balanced with N_2. In parallel experiments aimed at stimulating a restricted area of the muscle, and hence fewer capillary modules, animals were positioned on a smaller gas-exchange window (herein termed microwindow), measuring 200 by 400 μm. The gas chamber was fabricated and validated as previously described (9). This microwindow was covered by an O_2-permeable membrane made from polydimethylsiloxane (~60 μm thick; Sylgard™ 184 Silicone Elastomer, Dow Chemical Company). For measurement of normal capillary hemodynamics and standard constrictor/dilator experiments, the muscles were placed on a glass coverslip instead of the gas chamber and were otherwise treated as above. For these experiments, baseline recordings of the microcirculation were captured, followed by application of 10^{-4} M sodium nitroprusside, then 10^{-5} M phenylephrine HCl, followed by 10^{-3} M acetylcholine with a wash in between each drug application (Sigma-Aldrich). Throughout the surgical procedure and imaging, body temperature was monitored and maintained at 36.5 to 37.5 °C with a homeothermic heating pad system (Harvard Apparatus Canada).

Dual-Wavelength Intravital Video Microscopy. The EDL microvasculature was transilluminated with a 75-W xenon light source and imaged with an Olympus IX-81 inverted microscope (Olympus Corporation, Tokyo, Kanto, Japan). A 50/50 beam splitter (MAG Biosystems DC2 Dual-Channel, Full-Field, Simultaneous-Imaging System; Exton, PA, USA) divided light between two digital cameras (QImaging Rolera-XR FAST 1394 digital cameras; Surrey, BC, Canada). The beam splitter was fitted with 10-nm bandpass interference filters: one for 438-nm wavelength (hemoglobin O_2-dependent) and the other for 450-nm wavelength (isosbestic; hemoglobin O_2-independent), allowing for simultaneous dual-wavelength frame capture (696 × 520 pixel resolution; 21 frames/s) (54). The video sequences of microvascular networks were recorded for 6 min (7,560 frames) with a 450 × 340 μm field of view (FOV; 20 × long working distance objective). The frames were stored as 16-bit PNG files using custom acquisition software (Neovision, Prague, Czech Republic) and processed using in-house software written in MATLAB (MathWorks, Natick, MA, USA).

O_2 Challenge Protocol. O_2 at the muscle surface was changed by adjusting the O_2 flow through the gas chamber using computer-controlled mass flowmeters (Unit Instruments DX-5 Digital Control System and 7300 Mass Flow Controller/Meter, Kinetics, Yorba Linda, CA, USA). The DX-5 Digital Control System was driven by in-house software written in MATLAB. Chamber O_2 was measured in the gas outlet using a fiber optic PO_2 sensor connected to a spectrophotometer (USB2000 & USB-LS-450; Ocean Optics, Inc.). To perform a square-wave challenge (*SI Appendix*, Fig. S1*A*; red line), the muscle was exposed to 53 mmHg (7%; baseline) O_2 for one min and then to 15 mmHg (2%) O_2 for 3 min, followed by recovery at 53 mmHg O_2 for 2 min. With 53 mmHg O_2 in the chamber, the PO_2 is slightly above the physiological resting state in the tissue and 15 mmHg O_2 does not limit mitochondrial respiration in mouse skeletal muscle (20). The square wave was then repeated with 0% O_2 challenge (*SI Appendix*, Fig. S1*A*; dotted line). For a sine-wave challenge (*SI Appendix*, Fig. S1*B*), the chamber O_2 was set to 53 mmHg for 1 min and then oscillated at 1 cycle per min between 15 mmHg and 91 mmHg (12%) O_2 for 4 min, followed by recovery at 53 mmHg O_2 for 1 min. For a high O_2 challenge, the EDL was exposed to 53 mmHg O_2 for 1 min and then the O_2 level was increased to 91 mmHg for 3 min (or 152 mmHg; 20%), followed by recovery at 53 mmHg O_2 for 2 min.

Capillary Analysis. RBC flow through capillaries in each FOV was derived from automated frame-by-frame analysis as previously described (55). Briefly, functional images of each FOV were generated from the processed intravital microscopy frame sequences to distinguish columns of flowing RBCs from surrounding muscle fibers, allowing for capillary location and diameter to be determined. In-focus capillary segments were selected from these functional images and space-time images were generated from the light intensity along the centerline of each capillary segment, displaying the movement of RBCs, shown as tracts color-coded for O_2 saturation in Fig. 1. The space-time images were used to calculate capillary RBC dynamics. Specifically, RBC velocity (μm/s) was calculated from the spatial displacement of RBCs from frame to frame. Capillary hematocrit (%) was calculated as lineal density (RBC/mm) × RBC volume/capillary volume. RBC supply rate (RBC/s) was calculated as the product of RBC lineal density and velocity. The optical densities (ODs) for 450 nm and 438 nm were calculated using

the Beer–Lambert law–OD = log (I_0/I_{RBC}), where I_0 is incident light transmitted through plasma and I_{RBC} is light transmitted through an RBC. RBC hemoglobin SO_2 was derived from the calculated 438 nm/450 nm OD ratio with constants based on in vivo calibration and displayed in the space-time image (Fig. 1).

In Vivo Fluorescence Microscopy. Under urethane/α-chloralose anesthesia, C57BL/6 mice were prepared for in vivo imaging of the EDL microvasculature and injected with FITC-labeled dextran (2,000 kDa, 0.6 mg; Sigma-Aldrich) via the tail vein. The animals were placed on the microscope stage with the muscle positioned on a coverslip, covered with O_2-impermeable membrane, and imaged using a Nikon Ti2-E Confocal Inverted Microscope (Nikon Canada Inc., Mississauga, ON). 3D scans (150 to 200 μm thick) were acquired using the Nikon A1R HD resonant scanner. Arterial diameters were measured in the muscle at rest using NIS-Elements Software (Nikon).

Computational Modeling of Tissue PO_2 and Microvascular Blood Flow. A model of tissue O_2 transport supplied by capillaries was constructed, solved by a time-dependent finite-difference method, and modeled with spatially localized and fixed boundary conditions. An array of 72 uniformly spaced parallel capillaries embedded within a rectangular block of tissue was used to simulate tissue O_2 consumption, convective transport in the x direction (450 μm), and diffusive transport in z (200 μm) and y (500 μm). Muscle PO_2 in 3D was calculated with respect to how the steady-state value changes by 1) diffusive interactions with the gas chamber and 2) O_2-induced changes to RBC velocity, density, and SO_2.

For microvascular blood flow modeling, a steady-state, two-component (plasma and RBCs) phase separation model (56) was used to determine how RBCs distribute at diverging bifurcations for given blood flow fractions to the daughter branches. Precapillary arteriole diameters were measured in the EDL at rest (on cover glass) and based on these measurements, it was assumed that arterioles directly supplying stimulated capillary modules in the model have diameters of approximately 6 μm. Parent vessels were determined to be of this size or slightly larger, which is smaller than would be implied by extending Murray's Law (57) to arterioles. In addition, since very small arterioles have larger resistance than the capillary modules they supply, it was assumed that only very small diameter increases would be needed to increase flow ~10% as considered here. Therefore, diameter changes were not explicitly considered when applying the phase separation effect for increases in blood flow to these arterioles. Finally, blood (volume) flow was considered to represent measured RBC velocity, while RBC volume flow (blood flow times hematocrit) was considered to represent measured RBC supply rate.

Immunofluorescence Labeling of Cx37 and Cx40 in the EDL. C57BL/6 and *Cx40*$^{-/-}$ mice were overdosed with anesthesia, and the EDL muscles were extracted and placed in 4% paraformaldehyde at 4 °C until use. Muscles were pinned on Sylgard™ in multiwell plates and incubated in blocking buffer (PBS containing 1% normal donkey serum and 0.2% Tween 20) for 1 h at room temperature. After rinsing with PBS (3 × 5 min), muscles were incubated with anti-Cx37 and anti-Cx40 in blocking buffer (*SI Appendix*, Table S1) for 18 h at room temperature or for 36 h at 4 °C. Muscles were then rinsed in PBS (3 × 5 min) and incubated in secondary antibody diluted in 0.01% Tween 20 for 2 h. The muscles were splayed on microscope slides in anti-fade mounting media (buffered glycerol with ~1 mM propidium iodide) and imaged using a confocal microscope (FV1000; Olympus, Tokyo, Japan).

Statistical Analysis. Analysis was performed with GraphPad Prism version 9.2.0 (GraphPad Software; La Jolla, CA, USA). Capillary RBC supply rate, velocity, and hematocrit across the different O_2 challenges were categorized timewise as baseline, challenge time 1 and 2, and recovery (*SI Appendix*, Fig. S1*A*) and were normalized to the baseline measurement in each capillary. Capillary measurements were then averaged for each mouse to yield independent values. The D'Agostino and Pearson test was used to determine whether data are normally distributed. Significant differences between RBC flow at baseline and during an O_2 challenge with normally distributed data were determined with repeated measures one-way ANOVA with Šídák's multiple comparisons test. Significant differences between non-normally distributed data were determined using the Friedman test (repeated measures) with Dunn's multiple comparisons test. An unpaired *t* test (for parametric data) or unpaired Mann–Whitney test (for non-parametric data) was used to determine differences in capillary RBC velocity, hematocrit, RBC supply rate, and RBC SO_2 between control and knockout groups. Statistical significance was defined as $P < 0.05$.

Data, Materials, and Software Availability. Data that support the findings of this study are provided within this article and supplemental file.

ACKNOWLEDGMENTS. We thank Suzanne Brett and Michelle Kim (University of Western Ontario) for excellent animal care support. We also thank Richard Sové (Johns Hopkins University) for designing and validating the microwindow/O_2 exchange platform. This work was funded by the Canadian Institutes of Health Research to D.G., C.G.E., and D.G.W. (Grant # 453253). D.G.W. is the Rorabeck Chair in Vascular Biology and Neuroscience.

Author affiliations: [a]Robarts Research Institute, University of Western Ontario, London, ON N6A 5B7, Canada; [b]Department of Physiology and Pharmacology, University of Western Ontario, London, ON N6A 5B7, Canada; [c]Department of Medical Biophysics, University of Western Ontario, London, ON N6A 5B7, Canada; [d]School of Health, University of the Sunshine Coast, Maroochydore, QLD 4556, Australia; and [e]School of Clinical Medicine, University of Queensland, St. Lucia, QLD 4072, Australia

1. S. S. Segal, Regulation of blood flow in the microcirculation. *Microcirculation* **12**, 33–45 (2005).
2. J. A. Filosa *et al.*, Local potassium signaling couples neuronal activity to vasodilation in the brain. *Nat. Neurosci.* **9**, 1397–1403 (2006).
3. D. Goldman, Theoretical models of microvascular oxygen transport to tissue. *Microcirculation* **15**, 795–811 (2008).
4. T. L. Clanton, M. C. Hogan, L. B. Gladden, Regulation of cellular gas exchange, oxygen sensing, and metabolic control. *Compr. Physiol.* **3**, 1135–1190 (2013).
5. C. G. Ellis, S. Milkovich, D. Goldman, What is the efficiency of ATP signaling from erythrocytes to regulate distribution of O_2 supply within the microvasculature? *Microcirculation* **19**, 440–450 (2012).
6. M. L. Ellsworth *et al.*, Erythrocytes: Oxygen sensors and modulators of vascular tone. *Physiology* **24**, 107–116 (2009).
7. W. F. Jackson, Arteriolar oxygen reactivity: Where is the sensor and what is the mechanism of action? *J. Physiol.* **594**, 5055–5077 (2016).
8. N. W. Ghonaim, L. W. M. Lau, D. Goldman, C. G. Ellis, J. Yang, A micro-delivery approach for studying microvascular responses to localized oxygen delivery. *Microcirculation* **18**, 646–654 (2011).
9. R. J. Sové *et al.*, Localized oxygen exchange platform for intravital video microscopy investigations of microvascular oxygen regulation. *Front. Physiol.* **12**, 1–12 (2021).
10. G. M. Fraser, S. Milkovich, D. Goldman, C. G. Ellis, Mapping 3-D functional capillary geometry in rat skeletal muscle in vivo. *Am. J. Physiol. Circ. Physiol.* **302**, H654–H664 (2012).
11. J. S. Fang, S. N. Angelov, A. M. Simon, J. M. Burt, Cx40 is required for, and Cx37 limits, postischemic hindlimb perfusion, survival and recovery. *J. Vasc. Res.* **49**, 2–12 (2012).
12. T. A. Longden *et al.*, Capillary K^+-sensing initiates retrograde hyperpolarization to increase local cerebral blood flow. *Nat. Neurosci.* **20**, 717–726 (2017).
13. P. D. Smith *et al.*, K_{IR} channels function as electrical amplifiers in rat vascular smooth muscle. *J. Physiol.* **586**, 1147–1160 (2008).
14. S. K. Sonkusare, T. Dalsgaard, A. D. Bonev, M. T. Nelson, Inward rectifier potassium (Kir2.1) channels as end-stage boosters of endothelium-dependent vasodilators. *J. Physiol.* **594**, 3271–3285 (2016).
15. J. H. Lombard, B. R. Duling, Relative importance of tissue oxygenation and vascular smooth muscle hypoxia in determining arteriolar responses to occlusion in the hamster cheek pouch. *Circ. Res.* **41**, 546–551 (1977).
16. R. S. Richardson, E. A. Noyszewski, K. F. Kendrick, J. S. Leigh, P. D. Wagner, Myoglobin desaturation during exercise. *J. Clin. Invest.* **96**, 1916–1926 (1995).
17. F. M. Scandurra, E. Gnaiger, Cell respiration under hypoxia: Facts and artefacts in mitochondrial oxygen kinetics. *Adv. Experim. Med. Biol.* **662**, 7–25 (2010).
18. R. Bruzzone, J. A. Haefliger, R. L. Gimlich, D. L. Paul, Connexin40, a component of gap junctions in vascular endothelium, is restricted in its ability to interact with other connexins. *Mol. Biol. Cell* **4**, 7–20 (1993).
19. A. Zechariah *et al.*, Intercellular conduction optimizes arterial network function and conserves blood flow homeostasis during cerebrovascular challenges. *Arterioscler. Thromb. Vasc. Biol.* **40**, 733–750 (2020).
20. D. J. Marcinek, W. A. Ciesielski, K. E. Conley, K. A. Schenkman, Oxygen regulation and limitation to cellular respiration in mouse skeletal muscle in vivo. *Am. J. Physiol. Circ. Physiol.* **285**, H1900–H1908 (2003).
21. H. J. Knot, P. A. Zimmermann, M. T. Nelson, Extracellular K^+-induced hyperpolarizations and dilatations of rat coronary and cerebral arteries involve inward rectifier K^+ channels. *J. Physiol.* **492**, 419–430 (1996).
22. N. W. Ghonaim *et al.*, Evidence for role of capillaries in regulation of skeletal muscle oxygen supply. *Microcirculation* **28**, e12699 (2021).
23. C. L. Murrant, I. R. Lamb, N. M. Novielli, Capillary endothelial cells as coordinators of skeletal muscle blood flow during active hyperemia. *Microcirculation* **24**, 1–10 (2017).
24. H. H. Dietrich, K. Tyml, Capillary as a communicating medium in the microvasculature. *Microvasc. Res.* **43**, 87–99 (1992).
25. J. Yu, A. Bihari, D. Lidington, K. Tyml, Gap junction uncouplers attenuate arteriolar response to distal capillary stimuli. *Microvasc. Res.* **59**, 162–168 (2000).

26. G. S. Goldberg, A. P. Moreno, P. D. Lampe, Gap junctions between cells expressing connexin 43 or 32 show inverse permselectivity to adenosine and ATP. *J. Biol. Chem.* **277**, 36725–36730 (2002).
27. J. C. Saez, V. M. Berthoud, M. C. Branes, A. D. Martinez, E. C. Beyer, Plasma membrane channels formed by connexins: Their regulation and functions. *Physiol. Rev.* **83**, 1359–400 (2003).
28. Y. Yamamoto, M. F. Klemm, F. R. Edwards, H. Suzuki, Intercellular electrical communication among smooth muscle and endothelial cells in guinea-pig mesenteric arterioles. *J. Physiol.* **535**, 181–195 (2001).
29. A. P. Henriquez *et al.*, Influence of dynamic gap junction resistance on impulse propagation in ventricular myocardium: A computer simulation study. *Biophys. J.* **81**, 2112–2121 (2001).
30. M. J. A. van Kempen, H. J. Jongsma, Distribution of connexin37, connexin40 and connexin43 in the aorta and coronary artery of several mammals. *Histochem. Cell Biol.* **112**, 479–486 (1999).
31. F. Alonso *et al.*, An angiotensin II- and NF-κB-dependent mechanism increases connexin 43 in murine arteries targeted by renin-dependent hypertension. *Cardiovasc. Res.* **87**, 166–176 (2010).
32. A. Jobs *et al.*, Defective Cx40 maintains Cx37 expression but intact Cx40 is crucial for conducted dilations irrespective of hypertension. *Hypertension* **60**, 1422–1429 (2012).
33. H. Gu, F. C. Smith, S. M. Taffet, M. Delmar, High incidence of cardiac malformations in connexin40-deficient mice. *Circ. Res.* **93**, 201–206 (2003).
34. C. de Wit, F. Roos, S.-S. Bolz, U. Pohl, Lack of vascular connexin 40 is associated with hypertension and irregular arteriolar vasomotion. *Physiol. Genomics* **13**, 169–177 (2003).
35. N. Krattinger *et al.*, Connexin40 regulates renin production and blood pressure. *Kidney Int.* **72**, 814–822 (2007).
36. A. E. Chang, R. Detar, Oxygen and vascular smooth muscle contraction revisited. *Am. J. Physiol. Hear. Circ. Physiol.* **7**, H716–H728 (1980).
37. J. C. Frisbee, K. G. Maier, J. R. Falck, R. J. Roman, J. H. Lombard, Integration of hypoxic dilation signaling pathways for skeletal muscle resistance arteries. *Am. J. Physiol. Regul. Integr. Comp. Physiol.* **283**, 309–319 (2002).
38. E. J. Messina, D. Sun, A. Koller, M. S. Wolin, G. Kaley, Role of endothelium-derived prostaglandins in hypoxia-elicited arteriolar dilation in rat skeletal muscle. *Circ. Res.* **71**, 790–796 (1992).
39. E. J. Messina, D. Sun, A. Koller, M. S. Wolin, G. Kaley, Increases in oxygen tension evoke arteriolar constriction by inhibiting endothelial prostaglandin synthesis. *Microvasc. Res.* **48**, 151–160 (1994).
40. J. Tateishi, J. E. Faber, Inhibition of arteriole α_2- but not α_1-adrenoceptor constriction by acidosis and hypoxia in vitro. *Am. J. Physiol. Circ. Physiol.* **268**, H2068–H2076 (1995).
41. J. Tateishi, J. E. Faber, ATP-sensitive K^+ channels mediate α_{2D}-adrenergic receptor contraction of arteriolar smooth muscle and reversal of contraction by hypoxia *Circ. Res.* **76**, 53–63 (1995).
42. C. J. M. Kerkhof, E. N. T. P. Bakker, P. Sipkema, Role of cytochrome P-450 4A in oxygen sensing and NO production in rat cremaster resistance arteries. *Am. J. Physiol. Hear. Circ. Physiol.* **277**, 1546–1552 (1999).
43. C. H. T. Tran, E. J. Vigmond, D. Goldman, F. Plane, D. G. Welsh, Electrical communication in branching arterial networks. *Am. J. Physiol. Circ. Physiol.* **303**, H680–H692 (2012).
44. M. L. Ellsworth, T. Forrester, C. G. Ellis, H. H. Dietrich, The erythrocyte as a regulator of vascular tone. *Am. J. Physiol. Hear. Circ. Physiol.* **269**, H2155–H2161 (1995).
45. M. L. Ellsworth, C. G. Ellis, R. S. Sprague, Role of erythrocyte-released ATP in the regulation of microvascular oxygen supply in skeletal muscle. *Acta Physiol.* **216**, 265–276 (2016).
46. J. E. Jagger, R. M. Bateman, M. L. Ellsworth, C. G. Ellis, Role of erythrocyte in regulating local O_2 delivery mediated by hemoglobin oxygenation. *Am. J. Physiol. Circ. Physiol.* **280**, H2833–H2839 (2001).
47. R. M. Bateman, M. D. Sharpe, J. E. Jagger, C. G. Ellis, Sepsis impairs microvascular autoregulation and delays capillary response within hypoxic capillaries. *Crit. Care* **19**, 389 (2015).
48. P. M. Kowalewska *et al.*, Spectroscopy detects skeletal muscle microvascular dysfunction during onset of sepsis in a rat fecal peritonitis model. *Sci. Rep.* **12**, 6339 (2022).
49. K. Tyml, Role of connexins in microvascular dysfunction during inflammation. *Can. J. Physiol. Pharmacol.* **89**, 1–12 (2011).
50. K. Tyml, J. Yu, D. G. McCormack, Capillary and arteriolar responses to local vasodilators are impaired in a rat model of sepsis. *J. Appl. Physiol.* **84**, 837–844 (1998).
51. K. Tyml, X. Wang, D. Lidington, Y. Ouellette, Lipopolysaccharide reduces intercellular coupling in vitro and arteriolar conducted response in vivo. *Am. J. Physiol. Circ. Physiol.* **281**, H1397–H1406 (2001).
52. M. L. Bolon, T. Peng, G. M. Kidder, K. Tyml, Lipopolysaccharide plus hypoxia and reoxygenation synergistically reduce electrical coupling between microvascular endothelial cells by dephosphorylating connexin40. *J. Cell. Physiol.* **217**, 350–359 (2008).
53. P. M. Kowalewska *et al.*, Genetic ablation of smooth muscle $K_{IR}2.1$ is inconsequential to the function of mouse cerebral arteries. *J. Cereb. Blood Flow Metab.* **42**, 1693–1706 (2022).
54. T. Akerstrom *et al.*, Hyperinsulinemia does not cause de novo capillary recruitment in rat skeletal muscle. *Microcirculation* **27**, e12593 (2020).
55. G. M. Fraser, D. Goldman, C. G. Ellis, Microvascular flow modeling using in vivo hemodynamic measurements in reconstructed 3D capillary networks. *Microcirculation* **19**, 510–520 (2012).
56. A. R. Pries, T. W. Secomb, P. Gaehtgens, J. F. Gross, Blood flow in microvascular networks. *Circ. Res.* **67**, 826–834 (1990).
57. C. D. Murray, The physiological priniciple of minimum work: I. *Proc. Natl. Acad. Sci. U.S.A.* **12**, 207–214 (1926).